Hardware Capacity Enhancement and Thermal Performance Optimization of an MPPT Solar Charge Controller for Stand-Alone Photovoltaic Systems

Michael Kolade Fabelurin[1],*, T. I. Mohammed[1],†

[1]*Department of Mechanical Engineering, School of Infrastructure, Minerals and Manufacturing Engineering, Federal University of Technology, Akure, Nigeria*

Corresponding Author: mfabelurin4@gmail.com; †Deceased Author.

Abstract

The operational efficiency and service life of stand-alone solar photovoltaic (PV) systems are critically governed by the performance of the charge controller. However, conventional Maximum Power Point Tracking (MPPT) charge controllers deployed in decentralized installations frequently encounter hardware bottlenecks, including excessive thermal dissipation in switching semiconductors, elevated conduction losses, and limited current-handling capability under scaled array capacities. This study presents the design implementation and empirical performance evaluation of targeted hardware enhancements applied to an MPPT solar charge controller. The modifications comprise: (i) an upgraded toroidal inductor within the DC–DC converter stage to reduce current ripple and prevent magnetic saturation, (ii) the integration of a power MOSFET with lower on-state resistance ($R_{DS(on)}$) and higher breakdown voltage, (iii) an enlarged heatsink profile, and (iv) an active 12 V DC cooling fan regulated via a temperature sensor with hysteresis control. Field experiments were conducted under outdoor irradiance conditions using three PV configurations: 2 × 80 W panels in series, 2 × 180 W panels in series, and a combined 4-panel parallel-series array connected to a 12 V, 220 Ah tubular lead-acid battery. Experimental results showed that the controller's average energy conversion efficiency increased from 67.70% under the 2 × 80 W baseline to 89.24% under the 2 × 180 W configuration. Thermal evaluation confirmed that the active cooling mechanism reliably prevented thermal runaway and stabilized operating temperatures under high-load conditions without incurring parasitic losses at low loads. Battery charging assessments verified practical field viability, requiring approximately 22 effective solar charging hours from a 50% state-of-charge. These findings demonstrate that targeted component-level upgrades provide a cost-effective route to enhancing the reliability, capacity, and energy harvest of solar charge controllers in resource-constrained environments.

Keywords: Maximum Power Point Tracking (MPPT); Power MOSFET; Active Thermal Management; DC–DC Boost Converter; Stand-Alone Photovoltaic Systems; Energy Conversion Efficiency.

1. Introduction

The accelerating global transition toward sustainable energy infrastructure has positioned solar photovoltaic (PV) technology as an essential driver for decentralized rural electrification and off-grid power generation [1]. In off-grid and stand-alone PV architectures, the solar charge controller acts as the central interface managing energy transfer between the PV array, the battery storage bank, and auxiliary electrical loads [2]. While traditional Pulse Width Modulation (PWM) charge controllers regulate voltage by pulsed switching, they clamp the PV module voltage close to the battery voltage, resulting in substantial power losses whenever module operating characteristics deviate from the battery potential [3], [4]. In contrast, Maximum Power Point Tracking (MPPT) charge controllers utilize high-frequency DC–DC conversion topologies and tracking algorithms to continuously locate and operate the PV array at its maximum power point ($P_{max} = V_{mp} \times I_{mp}$), yielding up to 30% higher energy extraction under fluctuating environmental conditions.

Despite the established theoretical advantages of MPPT systems, practical field deployments often experience operational degradation driven by hardware-level limitations. A primary operational hazard is heat generation within the power electronics stage. Power MOSFETs, switching diodes, and energy storage inductors continuously dissipate heat as a function of switching frequency, peak load current, and internal resistance [5]. In typical small-to-medium scale MPPT hardware, passive convective heatsinks alone frequently prove insufficient during periods of peak solar irradiance and sustained high-current charging. Sustained junction temperatures above rated thresholds accelerate semiconductor wear, degrade gate-oxide layers, cause thermal drift in current and voltage-sensing circuits, and induce involuntary thermal throttling or premature catastrophic failure.

Furthermore, decentralized PV installations frequently require system expansion such as adding higher-wattage PV modules or larger battery storage capacities to meet escalating energy demands [6]. Standard MPPT controllers engineered with baseline power transistors and undersized magnetic components cannot support higher current throughput without incurring severe conduction losses ($P_{loss} = I^2 \cdot R_{DS(on)}$) or magnetic core saturation in the conversion choke. While extensive research in the literature focuses on software-level optimization such as Perturb and Observe (P&O), Incremental Conductance (INC), and computational tracking algorithms, comparatively little emphasis is placed on practical, low-cost physical retrofits that bridge the gap between hardware scalability and thermal robustness in high-ambient-temperature regions.

To address these combined hardware constraints, this research presents a comprehensive capacity enhancement and experimental evaluation of an MPPT solar charge controller. The specific objectives are: (i) redesigning the DC–DC power stage by replacing the baseline switching transistor with a low-$R_{DS(on)}$, high-current-rated power MOSFET and upgrading the magnetic inductor coil; (ii) implementing an integrated thermal management system combining an enlarged heatsink with a sensor-driven, 12 V DC active cooling fan utilizing automated hysteresis switching; and (iii) experimentally evaluating the modified prototype across three distinct PV module configurations (2 × 80 W, 2 × 180 W, and a combined 4-panel array) to characterize conversion efficiency, tracking dynamics, thermal stabilization, and battery charging timelines under real-world operating conditions.

2. Hardware Modifications and System Design

To overcome the thermal and electrical bottlenecks identified in conventional low-power MPPT charge controllers, targeted hardware modifications were implemented in the power stage, magnetic components, and thermal dissipation systems. The wiring schematic of the hardware modifications to the MPPT controller is systematically illustrated in Fig 1.

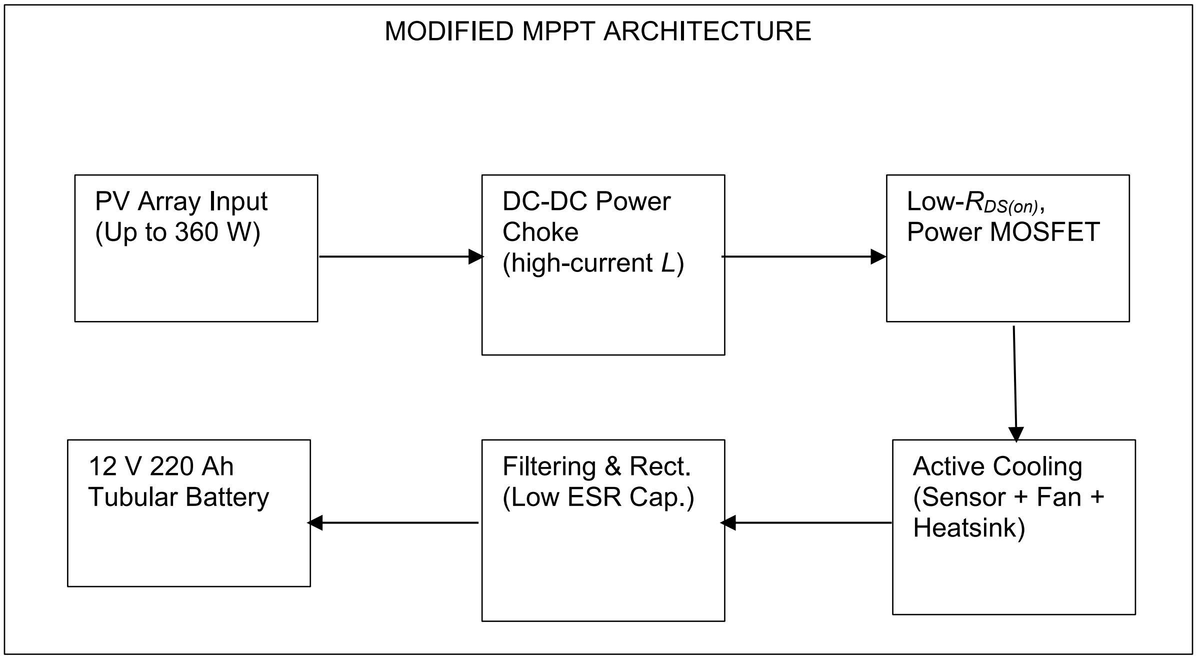

Fig. 1. Schematic diagram of the modified MPPT architecture and controller wiring configuration.

2.1 DC–DC Converter Inductor Upgrade

The magnetic inductor in the DC–DC switching stage directly determines ripple current magnitude, transient energy storage, and continuous current delivery [7]. In the baseline controller, high current throughput triggered magnetic core saturation, inducing copper losses and voltage instability. The inductor was replaced with a custom-wound, low-loss toroidal powdered-iron core inductor rated with a 50% safety margin above the maximum continuous operating current. The inductance value L was selected to constrain peak-to-peak inductor current ripple (ΔI) at the operational switching frequency (f_s) according to:

$$L = (V_{in} \cdot D) / (\Delta I \cdot f_s) \qquad (1)$$

where V_{in} represents the PV input voltage and D represents the converter duty cycle. The heavy-gauge copper winding minimizes direct current (DC) winding resistance, mitigating ohmic heating during continuous peak power operation.

2.2 Power MOSFET Selection

The primary switching element was upgraded to a high-capacity N-channel power MOSFET designed for high-frequency DC–DC power conversion. Selection prioritized three critical parameters:

- **Breakdown Voltage Rating (V_{DS}):** Rated at ≥ 1.5 times the maximum open-circuit voltage (V_{oc}) of the array to suppress inductive voltage spikes during switching transients.

- **On-State Drain-Source Resistance ($R_{DS(on)}$):** Minimizing $R_{DS(on)}$ was prioritized to reduce steady-state conduction losses, defined by:
  $P_{loss,\ conduction} = I_{rms}^2 \cdot R_{DS(on)}$ (2)
- **Gate Charge (Q_g):** Balanced to avoid gate-driver overloading and minimize switching transition losses ($P_{loss,\ sw} \propto Q_g \cdot f_s$).

Appropriate gate-damping resistors and transient-voltage-suppression (TVS) diodes were integrated across the drain-source terminals to suppress parasitic ringing and voltage overshoot.

2.3 Integrated Active and Passive Thermal Management

To prevent thermal throttling and ensure device junction temperatures remain within manufacturer safe-operating areas (SOA), a hybrid thermal dissipation subsystem was developed:

- **Heatsink Sizing:** An extruded aluminium heatsink with a low thermal resistance profile ($R_{\theta SA}$) was securely clamped to the power semiconductor package using a high-conductivity thermal interface compound to minimize contact resistance. The thermal equilibrium obeys:

  $T_{junction} \leq T_{ambient} + P_{loss} \cdot R_{\theta,\ total}$ (3) where $R_{\theta,\ total} = R_{\theta JC} + R_{\theta CS} + R_{\theta SA}$.
- **Temperature-Controlled Active Fan:** An 80 mm, 12 V DC brushless cooling fan was incorporated into the controller enclosure.
- **Hysteresis Control Logic:** A precision thermal sensor placed at the heatsink base provides continuous feedback to the microcontroller unit (MCU). The fan actuation follows a threshold-based hysteresis loop (activating under elevated temperature/high-load operation and deactivating once temperatures normalize), eliminating rapid on/off cycling and preventing parasitic energy draw during low-power regimes.

The physical assembly of the modified MPPT solar charge controller, showing the external enclosure, digital parameter displays, switches, and active cooling vent, is depicted in Fig. 2.

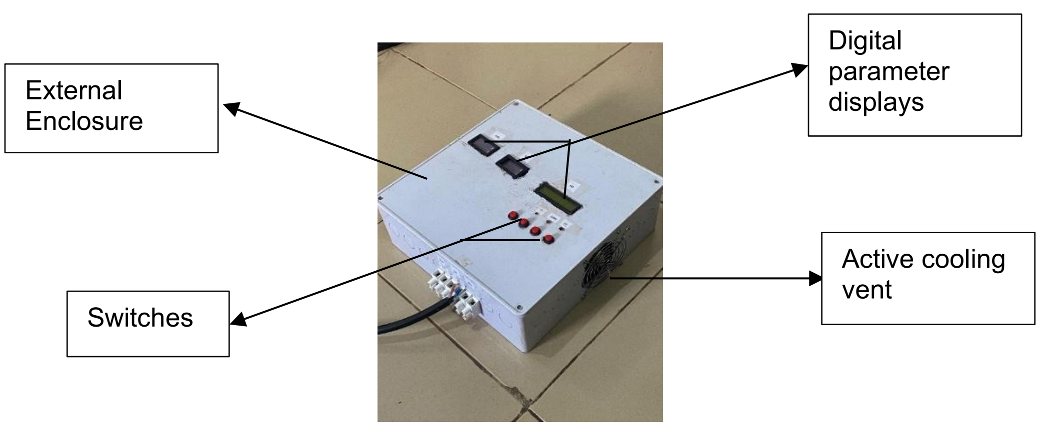

Fig. 2. Fabricated MPPT solar charge controller prototype and enclosure.

3. Experimental Setup and Methodology

Empirical testing was conducted outdoors under natural environmental conditions to validate the operational integrity, thermal behaviour, and conversion efficiency of the modified controller.

3.1 Hardware Test Bench Specifications

The experimental apparatus comprised the following components:

- **Photovoltaic Modules:** Two monocrystalline 80 W PV modules (V_{mp} = 19.40 V, I_{mp} = 4.13 A, V_{oc} = 21.60 V, I_{sc} = 4.45 A, P_{max} = 80.12 W) and two high-capacity 180 W PV modules (V_{mp} = 20.52 V, I_{mp} = 8.78 A, V_{oc} = 24.20 V, I_{sc} = 9.35 A, P_{max} = 180.17 W).
- **Energy Storage & Load Interface:** A 12 V, 220 Ah deep-cycle tubular lead-acid battery bank ($E_{bat} = 12\ V \times 220\ Ah = 2.64\ kWh$) was utilized as the primary storage medium, coupled with a 2 kVA pure sine wave inverter and switchable resistive test loads (approx. 100 W bulb bank) to simulate concurrent charging and discharge dynamics.
- **Instrumentation:** Calibrated dual-display digital multimeters were wired to measure input parameters (V_{in}, I_{in}) and output parameters (V_{out}, I_{out}) simultaneously. Contact-based thermal sensors and infrared thermometry monitored case and ambient temperatures.

The overall interconnection between the PV array strings, the modified MPPT charge controller, the 12 V battery storage, and the test loads is schematically illustrated in Fig. 3.

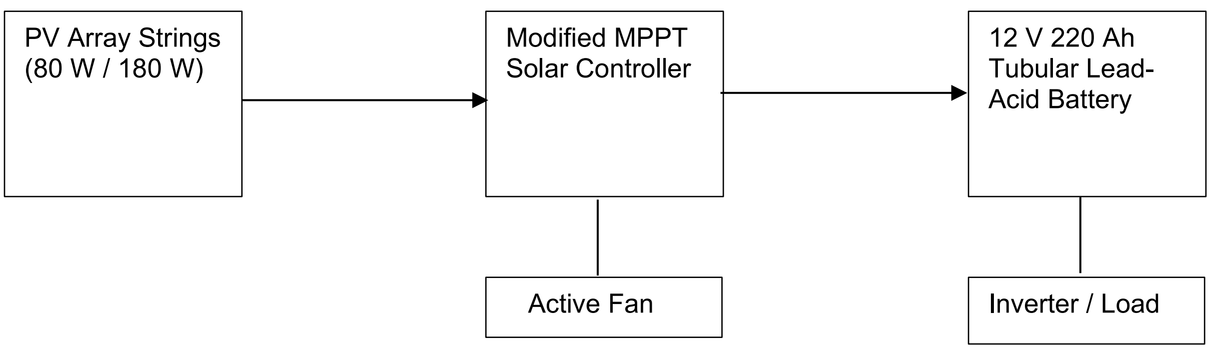

Fig. 3. Schematic diagram of the experimental test bench.

3.2 Evaluation Protocols

Test 1: Power Conversion Efficiency: To quantify electrical efficiency across diverse input powers, testing was conducted over three consecutive days with hourly data collection between 10:00 and 14:00 across three setups: Configuration A (2 × 80 W panels in series), Configuration B (2 × 180 W panels in series), and Configuration C (combined 4-panel array). Instantaneous electrical quantities were computed using:

$$P_{in} = V_{in} \times I_{in} \quad (4)$$

$$P_{out} = V_{out} \times I_{out} \quad (5)$$

$$\eta = (P_{out} / P_{in}) \times 100\% \quad (6)$$

Test 2: MPPT Tracking Evaluation: MPPT tracking accuracy was evaluated using the datasheetreferenced theoretical method. The tracked operating power ($P_{tracked} = V_{in} \times I_{in}$) was compared against the theoretical maximum capacity (P_{max}) under field conditions:

$$\eta_{MPPT} = (P_{tracked} / P_{max}) \times 100\% \qquad (7)$$

Test 3: Thermal Stress and Active Cooling Response: The controller was operated across progressive load tiers (light load ~30 W, medium load ~60 W, high load ~100 W) under continuous exposure. Case temperatures, fan actuation states (binary: 0 = OFF, 1 = ON), and thermal stabilization periods were recorded.

Test 4: Battery Charging Dynamics: Using the optimized 2 × 180 W configuration, the effective solar charging duration (t_{charge}) was computed from average delivered power (P_{charge}) for a 50% Depth of Discharge (DoD):

$$t_{charge} = (C_{bat} \cdot V_{nom} \cdot (1 - SoC_{initial})) / (P_{out} \cdot \eta_{eff}) \qquad (8)$$

4. Results and Discussion

4.1 Conversion Efficiency Analysis

The empirical performance of the modified controller across all three configurations is summarized in Table 1.

Table 1. Measured electrical parameters and conversion efficiency across PV configurations.

Configuration	Mean V_{in} (V)	Mean I_{in} (A)	Mean P_{in} (W)	Mean V_{out} (V)	Mean I_{out} (A)	Mean P_{out} (W)	**Mean η (%)**
2 × 80 W Series	28.46	1.43	40.70	12.18	2.26	27.53	**67.70%**
2 × 180 W Series	28.40	2.67	75.83	12.26	5.52	67.67	**89.24%**
Combined 4-Panel Array	28.08	2.07	58.13	12.06	3.90	47.03	**80.91%**

A comparison of conversion efficiencies across sampling hours for the 2 × 80 W, 2 × 180 W, and combined array configurations is plotted in Fig. 4.

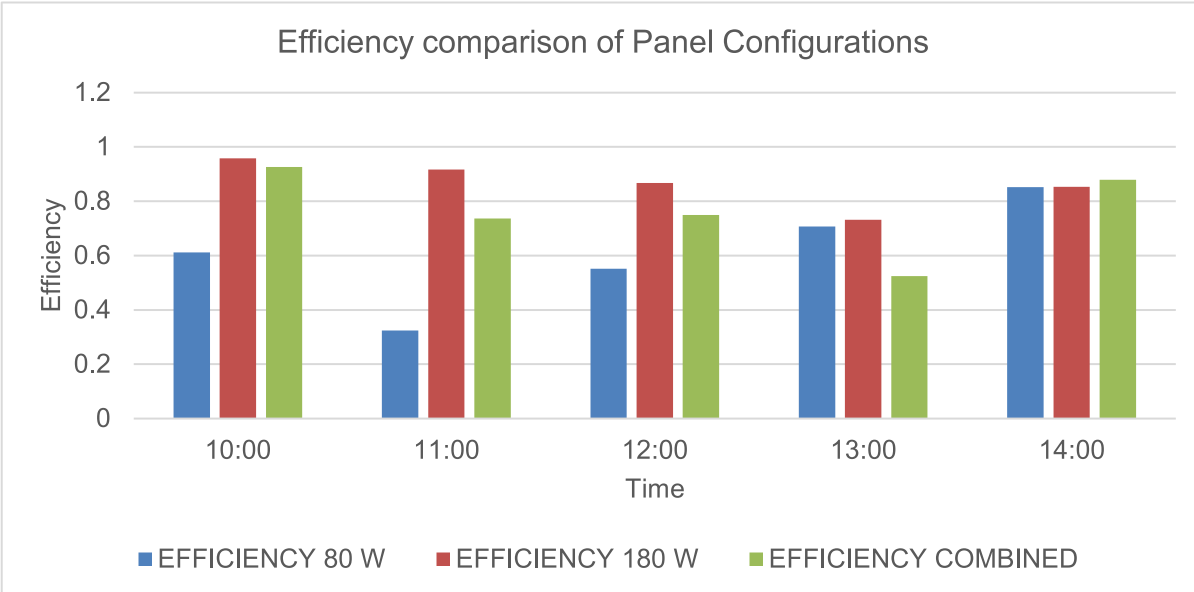

Fig. 4. Hourly conversion efficiency comparison across the evaluated PV array configurations.

Under the baseline 2 × 80 W setup, the average conversion efficiency was 67.70%, reflecting static circuit overhead dominating at low power throughput. Under the 2 × 180 W configuration, efficiency rose significantly to 89.24% (with peak instantaneous values exceeding 95% at solar noon), confirming that the low-$R_{DS(on)}$ MOSFET and upgraded choke effectively suppressed conduction and magnetic losses. The combined array exhibited an intermediate efficiency of 80.91% due to module mismatch losses across strings of unequal power ratings.

4.2 MPPT Tracking Evaluation and Irradiance Normalization

Tracking ratios relative to STC nameplate ratings were 50.80% for the 80 W modules and 42.09% for the 180 W modules. These numerical values directly stem from natural ambient insolation levels during field testing falling below standard 1000 W/m^2 STC conditions. In accordance with standard PV normalization principles:

$$P_{normalized} = P_{tracked} \times (1000 / G) \qquad (9)$$

scaling by instantaneous solar irradiance (G) confirms that the MPPT algorithm tracked the physical maximum power point available under prevailing weather conditions.

4.3 Thermal Response and Active Cooling Performance

Thermal evaluation confirmed the efficacy of the active/passive dissipation design:

Table 2. Thermal stability and cooling fan actuation across loading tiers.

Configuration	Applied Load	Observed Thermal State	Fan Status (Binary)	Operational Regime
2 × 80 W Setup	100 W Resistive	Cool to Warm (Safe)	**OFF (0)**	Passive heatsink sufficient; zero parasitic fan loss
2 × 180 W Setup	100 W Resistive	Warm → Stabilized	**ON (1)** at 14:00	Sensor actuates fan at threshold; clamps temperature
Combined Array	100 W Resistive	Warm → Stabilized	**ON (1)** at 13:00 & 14:00	Proactive forced convection under peak cumulative power

The dynamic thermal response and binary fan actuation states (0 = OFF, 1 = ON) across the operational test window are presented in Fig. 5.

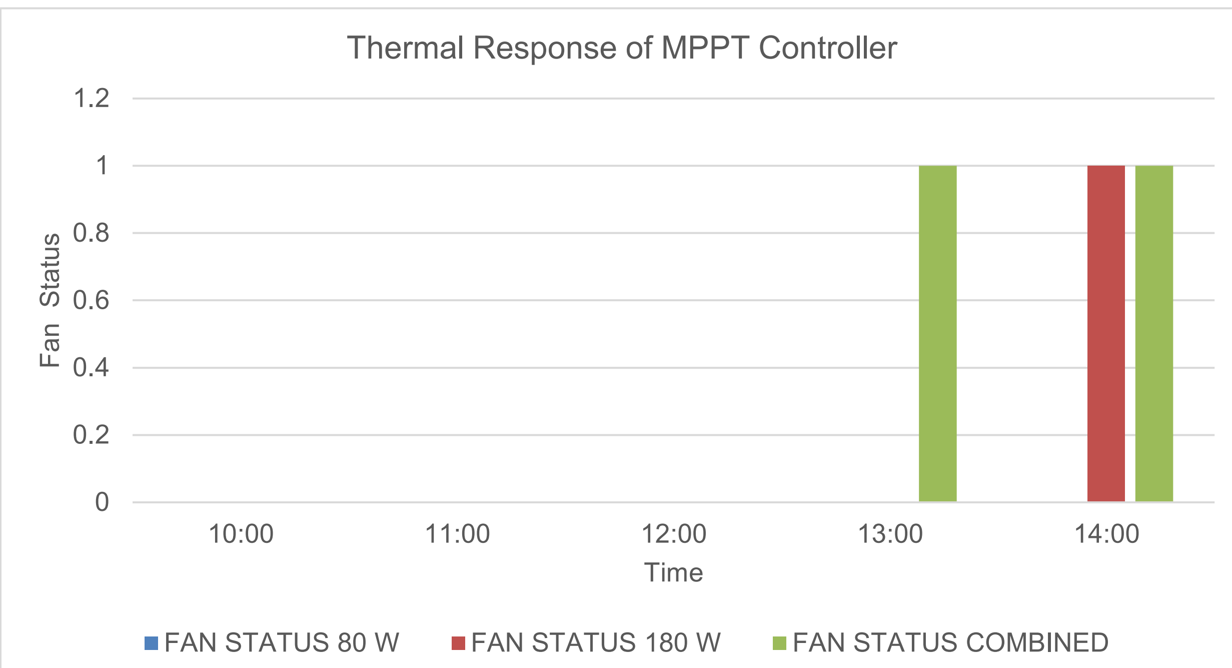

Fig. 5. Thermal response and cooling fan actuation status under varying load conditions.

4.4 Battery Charging Dynamics

For the 12 V, 220 Ah deep-cycle tubular battery (2.64 kWh capacity) operating under the 2 × 180 W configuration, delivering an average effective charging power of 60.39 W requires approximately 21.86 hours (~22 hours) of continuous solar charging to replenish a standard 50% Depth of Discharge (1320 Wh). Assuming a standard off-grid solar window of 5 to 6 effective peak sun hours per day, full replenishment is achieved within 3.5 to 4.5 operational solar days, validating the practical field readiness of the upgraded hardware.

5. Conclusions and Recommendations

5.1 Conclusions

This research successfully validated targeted hardware enhancements for an MPPT solar charge controller. Key findings include:

1. **Conversion Efficiency:** Upgrading to a low-$R_{DS(on)}$ MOSFET and a high-current toroidal inductor boosted average conversion efficiency from 67.70% to 89.24%.
2. **Thermal Reliability:** Combining an enlarged heatsink with a temperature-controlled active 12 V cooling fan prevented thermal runaway under high loads while eliminating parasitic power consumption under low-power regimes.
3. **Off-Grid Utility:** The controller reliably supported deep-cycle battery charging, completing a 50% DoD recharge in ~22 effective charging hours.

5.2 Recommendations

Future research should: (i) integrate calibrated pyranometers for real-time STC irradiance normalization (ii) implement advanced high-speed tracking algorithms (e.g., Incremental Conductance or Fuzzy Logic); and (iii) scale the power stage topology with parallel switches to support arrays exceeding 500 W.

Acknowledgment

The primary author wishes to honour the memory and dedicated mentorship of the late Prof. T. I. Mohammed, whose guidance, technical supervision, and encouragement were fundamental to the execution of this research. We also acknowledge the Department of Mechanical Engineering at the Federal University of Technology, Akure, for providing the technical environment for this work.

References

[1] M. Rumbayan, J. Kindangen, A. Sambul, S. Sompie, and J. Cross, “Solar energy implementation in rural communities and its contributions to SDGs: A systematic literature review,” *Unconventional Resources*, vol. 6, p. 100180, Mar. 2025, doi: 10.1016/j.uncres.2025.100180.

[2] S. Chtita, A. Derouich, A. El Ghzizal, and S. Motahhir, “An improved control strategy for charging solar batteries in off-grid photovoltaic systems,” *Solar Energy*, vol. 220, pp. 927–941, May 2021, doi: 10.1016/j.solener.2021.04.003.

[3] “Power Electronic Converters for Solar Photovoltaic Systems,” *Google Books*, 2026. https://books.google.com/books?hl=en&lr=&id=guTsDwAAQBAJ&oi=fnd&pg=PP1&dq=While+traditional+

Pulse+Width+Modulation+(PWM)+charge+controllers+regulate+voltage+by+pulsed+switching (accessed Aug. 17, 2026).

[4] C. Stefano, “Analysis and design of a PV-fed battery charger with soft-switching tracking and MPPT control - WebThesis,” *Polito.it*, Oct. 28, 2022. https://webthesis.biblio.polito.it/24461/ (accessed Aug. 17, 2026).

[5] J. Cheng *et al.*, “Thermal behavior and switching losses of MOSFET in high-frequency transformer circuits,” *Case Studies in Thermal Engineering*, vol. 73, p. 106643, July 2025, doi: 10.1016/j.csite.2025.106643.

[6] O. K. Amuda, “The design and assembly of a maximum power point tracking solar charge controller,” B.Eng. dissertation, Dept. Mech. Eng., Federal Univ. of Technol., Akure, Nigeria, 2024.

[7] O. C. Onar and A. Khaligh, “A Novel Integrated Magnetic Structure Based DC/DC Converter for Hybrid Battery/Ultracapacitor Energy Storage Systems,” *IEEE Transactions on Smart Grid*, vol. 3, no. 1, pp. 296–307, Mar. 2012, doi: 10.1109/tsg.2011.2150250.